Letter

Precision measurement of $^{25}Mg^+$-ion D_1 and D_2 transition frequencies

P. Hao,[1] K. Deng,[1,*] F. F. Wu,[1] Z. Y. Ma,[1] W. Z. Wei,[1] W. H. Yuan,[1] Y. B. Du,[2] H. L. Liu,[1] H. X. Zhang,[1] L. R. Pang,[1] B. Wang,[1] J. Zhang,[1] and Z. H. Lu[1,†]

[1]*MOE Key Laboratory of Fundamental Physical Quantities Measurement, Hubei Key Laboratory of Gravitation and Quantum Physics, PGMF and School of Physics, Huazhong University of Science and Technology, Wuhan 430074, China*

[2]*MOE Key Laboratory of TianQin Mission, TianQin Research Center for Gravitational Physics & School of Physics and Astronomy, Frontiers Science Center for TianQin, CNSA Research Center for Gravitational Waves, Sun Yat-sen University (Zhuhai Campus), Zhuhai 519082, China*

(Received 27 June 2022; revised 8 September 2022; accepted 17 February 2023; published 27 February 2023)

Precision measurement of Mg^+ ion D_1 and D_2 doublet transition frequencies plays a significant part in the study of space-time variation of fundamental physical constant α. Here, we report a precision measurement of $^{25}Mg^+$ ion D_1 and D_2 doublet transition frequencies using the decoherence-assisted spectroscopy method with the full use of spontaneous emission signals to improve the detection sensitivity. We obtain the D_1 and D_2 transition frequencies of $^{25}Mg^+$ with uncertainties of 0.12 and 0.24 MHz, respectively, which are one third of that in [A. Ozawa *et al.*, Nat. Commun. **8**, 44 (2017)]. Simultaneously, we obtain the experimental and theoretical values of the $^{25}Mg^+$ hyperfine structure constants in this work. The differences between the measured magnetic dipole constants $A_{P_{1/2}} = -102.87(8)$ MHz, $A_{P_{3/2}} = -18.74(9)$ MHz and the theoretical values $A_{P_{1/2}} = -102.02(94)$ MHz, $A_{P_{3/2}} = -19.46(45)$ MHz are within 2σ, while the measured electric quadrupole constant $B_{P_{3/2}} = 24.54(45)$ MHz and the theoretical value of $B_{P_{3/2}} = 22.67(32)$ MHz shows a difference of more than 2σ, indicating that considerations of more physical effects in theoretical calculation, such as the possible capture of electron correlations, is required.

DOI: 10.1103/PhysRevA.107.L020803

Precision spectroscopy plays an important role in the study of space-time variation of fundamental physical constants [1–11]. Based on the comparison of the absorption spectra of quasars in the universe and those on the earth, scientists can search for the space-time variation of fine structure constant α [1–4]. In the meantime, the atomic transitions can also be used to study the isotope shift theory [12,13]. In particular, nonlinear isotope shift has been introduced to find new physics beyond the standard model [13–19].

The alkali-doublet (AD) method [1,2] was first introduced to constrain the time variation of α in comparison of the absorption spectra of quasars, where the Mg^+ ion doublet lines were used to give the upper limit on the variation of α. Later, the many-multiplet (MM) method [3,4] was introduced with higher sensitivity gain compared to the AD method, in which Mg^+ ion doublet lines act as anchor lines in the Mg II/Fe II system. This method allows one to use more quasar absorption lines and introduce relativistic corrections. As a consequence, precision measurement of the Mg^+ doublet lines plays an important role in the large space-time scale searching of the α variance. The laboratory results of these lines require the accuracy to be better than 10^{-4} Å [9], corresponding to an uncertainty below 40 MHz for 280 nm transition. Various uncertainty contributions need to be evaluated, such as absorption system model nonuniqueness, statistical uncertainty, absorption profile modeling uncertainty, isotopic relative abundances, and so on [20,21]. If these uncertainties can be improved in the future, the search for the possible variations of α would need laboratory results with higher precision. There are three stable isotopes of magnesium with mass numbers of 24, 25, and 26 (natural abundances of 79%, 10%, and 11%, respectively). The isotope shift and isotopic abundances measured on the earth are helpful to evaluate the isotopic and hyperfine structure effects in the absorption spectra of quasars [22,23].

The doublet transitions of Mg^+ ion have been measured in Penning traps [24–26] and in hollow-cathode lamps [27–29], with measurement uncertainties at tens of MHz. A sympathetically cooled ions chain in a linear Paul trap has been introduced to obtain symmetric line profiles, and the reported uncertainty of the $^{24,26}Mg^+$ transition is 0.16 MHz [30,31]. For $^{25}Mg^+$, it has a hyperfine structure with a nonzero nuclear magnetic moment ($I = \frac{5}{2}$). The low-lying excited state hyperfine constants have been theoretically calculated by several groups [32–35], and a recent experiment has reported the value of the magnetic dipole constant of $A_{P_{1/2}} = -102.16(16)$ MHz [36]. In this work, we have further reduced the measurement uncertainty. The ground-state magnetic dipole hyperfine constant has been measured in laboratory [37–39], and the latest result is $A_{S_{1/2}} = -596\,254\,250.949(45)$ Hz [39]. Due to the hyperfine structure, the $^{25}Mg^+$ ion doublet lines are more

*ke.deng@hust.edu.cn
†zehuanglu@hust.edu.cn

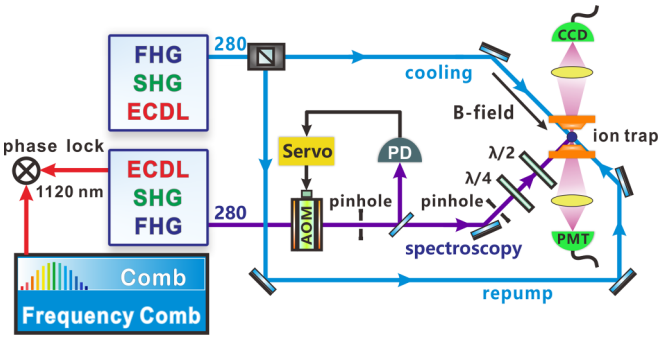

FIG. 1. Schematic of the experiment setup. The 280-nm FHG laser along the B-field direction is used for Doppler cooling and fluorescence detection. The second 280-nm laser serving as the spectroscopy laser travels perpendicular to the B-field direction, and is locked to a frequency comb that is referenced to a hydrogen maser. A photomultiplier tube (PMT) is used to count the photon number.

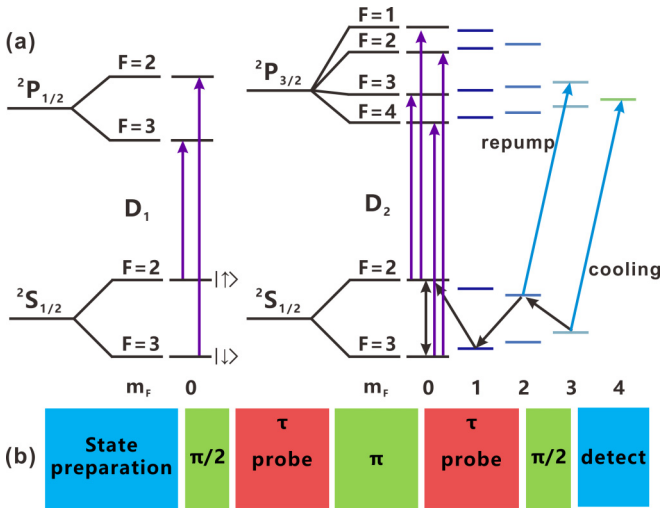

FIG. 2. (a) The energy levels of $^{25}Mg^+$. All the hyperfine transitions we measured are initiated from the ground state $|\uparrow\rangle$ or $|\downarrow\rangle$. The spectroscopy laser is set at π polarization, so the ions in the excited states will decay to other Zeeman sublevels of the ground state, losing coherence during the process. (b) Procedures of decoherence-assisted laser spectroscopy. Microwave pulses are used to create a spin echo sequence between $|\uparrow\rangle$ and $|\downarrow\rangle$ states. In between the microwave pulses, π polarized laser probe pulses with duration τ are introduced to create decoherence effects, from which the doublet transition frequencies can be determined.

difficult to measure directly. In a recent experiment [40], an ultraviolet (UV) frequency comb was used to detect the Zeeman sublevel cycling transitions of the $^{25}Mg^+$ ion. With the knowledge of the hyperfine structure constants [34,37], the D_2 transition frequency was given with an uncertainty of 0.7 MHz.

Recently, the $^{25}Mg^+$ ion doublet hyperfine transition lines were directly measured with a decoherence-assisted method [41] with an uncertainty of 5 MHz. It is limited by the probe laser linewidth, frequency measurement accuracy, and the other systematic effects.

In this paper, the $^{25}Mg^+$ ion doublet transition frequencies are measured with several improvements. We simulate the interaction between the laser and the ion to understand the main systematic error sources. The excited state hyperfine structure constants and the fine-structure transition frequencies of $^{25}Mg^+$ ion are measured with higher accuracy, in which the signal-to-noise ratio (SNR) is increased three times by optional state preparations. Simultaneously, we can also obtain the isotope shifts of the three isotopes of the Mg^+ ion.

The details of the $^{25}Mg^+$ ion trap system have been reported in Refs. [42,43], and we only give a brief description here. A single $^{25}Mg^+$ ion is trapped in a linear Paul trap with a 24 MHz driving frequency. Three pairs of coils outside the vacuum chamber are used to compensate for the external magnetic field and provide a constant bias field of $B \approx 2.24$ G. The magnetic field is measured with the transition ($^2S_{1/2}|3,3\rangle \rightarrow {}^2S_{1/2}|2,2\rangle$) of a single $^{25}Mg^+$ ion in the center of the trap, and the magnetic field noise is suppressed to less than 100 μG over a time period of 6000 s [44].

The schematic of our experimental setup is shown in Fig. 1. Two 280-nm fourth harmonic generation (FHG) laser systems (with the oscillator wavelength at 1120 nm) are used; one of them is used for the Doppler cooling and fluorescence detection, and the other is used as the spectroscopy laser. If we scan the laser frequency (∼400 MHz) with an acousto-optic modulator (AOM), it could cause large power variation, laser beam profile distortion, and change of laser beam direction, which would cause measurement uncertainties. Consequently, we choose to tune the piezoelectric transducer (PZT) on the laser oscillator to suppress these effects. In our case, the laser oscillator output passed through the fiber amplifier, the second harmonic generation (SHG) cavity, and the FHG cavity, which all serve as spatial filtering for the laser out. When the frequency of the rf source is changed, the voltage on the PZT will follow that change to ensure the beat signal is locked to a fixed 20 MHz signal whose reference is a hydrogen maser. We measure the beat-note linewidth of the laser and the optical frequency comb, in which the linewidth of the frequency comb is measured to be 0.19(1) MHz by beating with an ultrastable laser with subhertz linewidth [45]. The beat-note linewidth is evaluated to be 0.4(1) MHz at 1120 nm, which is limited by the servo loop bandwidth of about 2 kHz. We measure the laser beam profile with the knife-edge method to ensure that a Gaussian distribution of the beam profile is obtained. One part of the spectroscopy laser is split by a 50:50 beam splitter and used for laser power stabilization with a digital locking system.

The $^{25}Mg^+$ energy levels are shown in Fig. 2(a). A single $^{25}Mg^+$ ion is cooled to the Doppler cooling limit and first prepared to the state $^2S_{1/2}|F=3, m_F=3\rangle$ (in the following, it is written as $^2S_{1/2}|3,3\rangle$ for simplicity). In our experiment, we define the population on $^2S_{1/2}|2,2\rangle$ and $^2S_{1/2}|3,3\rangle$ state as the fluorescence bright and dark states. The average detected photon numbers at dark and bright states are 0.6 and 8.5 with a gate time of 100 μs. For the spectroscopy experiment, we further prepare the ion to either $^2S_{1/2}|2,0\rangle$ or $^2S_{1/2}|3,0\rangle$ (labeled as $|\uparrow\rangle$ and $|\downarrow\rangle$, respectively) using multiple microwave π pulses ($^2S_{1/2}|3,3\rangle \rightarrow |2,2\rangle \rightarrow |3,1\rangle \rightarrow |2,0\rangle$ or $^2S_{1/2}|3,3\rangle \rightarrow |2,2\rangle \rightarrow |3,1\rangle \rightarrow |2,0\rangle \rightarrow$

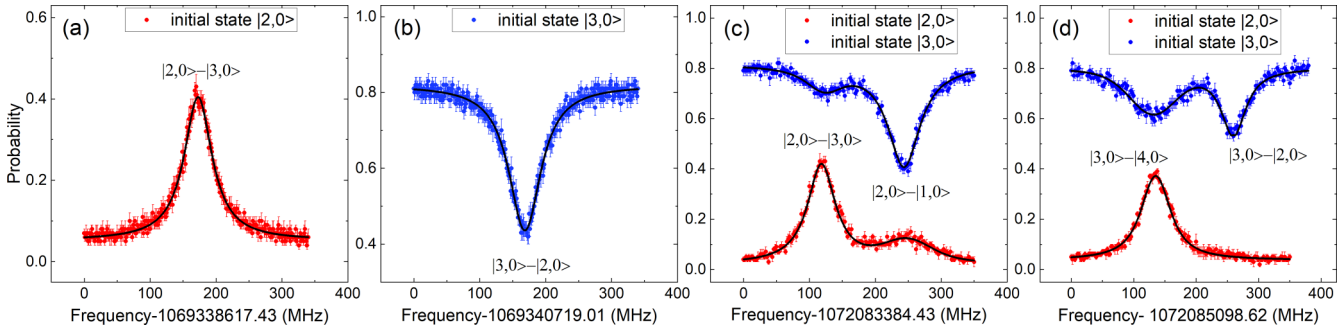

FIG. 3. $^{25}Mg^{+}$ ion D_1 and D_2 transition lines; solid lines are the Voigt profile fitting. The ions are prepared to different initial states (red data points: $|\uparrow\rangle$, blue data points: $|\downarrow\rangle$) to obtain higher SNR signals. (a) The $^2S_{1/2}\,|2,0\rangle \rightarrow\ ^2P_{1/2}|3,0\rangle$ transition spectrum. (b) The $^2S_{1/2}\,|3,0\rangle \rightarrow ^2P_{1/2}|2,0\rangle$ transition spectrum. (c) For the red data, the SNR of the $^2S_{1/2}\,|2,0\rangle \rightarrow\ ^2P_{3/2}|3,0\rangle$ at the left side of the spectrum is about three times higher than the blue data at the left side, while for the blue data $^2S_{1/2}\,|2,0\rangle \rightarrow\ ^2P_{3/2}|1,0\rangle$ at the right side of the spectrum, the SNR is three times better than that in the red data. (d) For the red data $^2S_{1/2}\,|3,0\rangle \rightarrow\ ^2P_{3/2}|4,0\rangle$ at the left side of the spectrum is about three times higher than the left side of the blue data, while for the right side of the blue data $^2S_{1/2}\,|3,0\rangle \rightarrow\ ^2P_{3/2}|2,0\rangle$, the SNR has been improved more than three times than that in the red data.

$|3,0\rangle$). The achieved population probabilities are 0.91(3) at $|\uparrow\rangle$ and 0.88(4) at $|\downarrow\rangle$, respectively.

As shown in Fig. 2(b), we introduce π polarized laser probe pulses with a duration $\tau = 350$ μs into the microwave spin echo sequence between the $|\uparrow\rangle$ and $|\downarrow\rangle$ states. If the laser frequency is far detuned from the doublet line transition frequencies, the population will remain in the initial state after the spin echo sequence. If the laser frequency is near resonant with the doublet line transitions, it will cause the populations to decay to other ground state energy levels, introducing the decoherence effect. If we directly detect the fluorescence signals during the doublet spectroscopy laser-ion action, the emissions from the different excited states to the same ground state would induce frequency shift due to the quantum interference effect [46,47]. In the decoherence-assisted spectroscopy method, after the populations decay to $^2S_{1/2}\,|F=2\rangle$ and $^2S_{1/2}\,|F=3\rangle$ and the last $\pi/2$ microwave pulse, all the populations on the Zeeman sublevels of $^2S_{1/2}\,|F=3\rangle$ are detected as signals—an advantage of this method where the coherent effect is largely suppressed. This method could avoid the frequency shift caused by quantum interference effect since all 4π solid angle spontaneous emissions are accounted for.

For D_2 transitions, the spectroscopy laser intensity is set to be $I_{\text{probe}} = 0.13(2)$ W/m^2, corresponding to a saturation parameter $s = 5(1) \times 10^{-5}$. The measured transition lines are shown in Fig. 3. Each point is repeated 1000 times within about 2.5 s, in which the error bars represent the statistical uncertainties, and the full scan of each transition line requires about 860 s. These transition lines are fitted with Voigt profiles, whose free-fitting parameters are the probability offset, the transition amplitude, the center frequency, the Lorentzian width Γ_{L}, and the Gaussian width Γ_{G}, and we have taken the Zeeman sublevel transitions into account. The fitted Lorentzian linewidth is $\Gamma_{\text{L}} = 2\pi \times 48(3)$ MHz, in which the natural linewidth contribution is $2\pi \times 41.8(4)$ MHz [48]. The intensity of the laser and the long probe time τ can homogeneously broaden the transition lines, and the simulated Lorentzian linewidth is $\Gamma_{\text{L}} = 2\pi \times 48.6(3)$ MHz, which agrees with the experimental linewidth. The fitted Gaussian linewidth is $\Gamma_{\text{G}} = 2\pi \times 12(4)$ MHz. The ion is initially cooled close to the Doppler cooling limit $T \approx 1$ mK, which corresponds to a width of $\Gamma_{\text{Doppler}} \approx 2\pi \times 5$ MHz. Further heating might afterwards broaden the linewidth.

According to the diagram in Fig. 2(a), if the ion is initially in state $|\uparrow\rangle$, for the transition between $|\uparrow\rangle$ and $^2P_{3/2}\,|3,0\rangle$, it could easily decay to other Zeeman sublevels of $^2S_{1/2}\,|F=2\rangle$ and $^2S_{1/2}\,|F=3\rangle$, causing a large decoherence signal. On the other hand, for the transition between $|\uparrow\rangle$ and $^2P_{3/2}\,|1,0\rangle$, there is no spontaneous emission to $^2S_{1/2}\,|F=3\rangle$, causing a weak decoherence signal. The result is shown as the bottom red curve in Fig. 3(c). If instead, we prepare the initial state to $|\downarrow\rangle$, when the spectroscopy laser is far detuned from the resonant frequency, it would remain in the initial state $|\downarrow\rangle$, which will be detected as the bright signal. When the laser frequency is near resonant, the signal radiated to each sublevel of $^2S_{1/2}\,|F=2\rangle$ will be detected as a dark signal, so that we can obtain a strong decoherence signal. The result is shown as the top blue curve in Fig. 3(c). Similarly, the SNR of the transition between $|\downarrow\rangle$ and excited state $^2P_{3/2}\,|2,0\rangle$ can be improved by more than three times with the initial state $|\downarrow\rangle$ instead of $|\uparrow\rangle$, and the transition between $|\downarrow\rangle$ and $^2P_{3/2}\,|4,0\rangle$ is detected with the prepared initial state $|\uparrow\rangle$ to obtain a three times higher SNR than the initial state at $|\downarrow\rangle$. The results are shown in Fig. 3(d). We compare the expected signal amplitudes for different initial prepared states through numerical simulation. The results are presented in the Supplemental Material [49] and agree well with our experimental results. The simulation shows that the SNR can be improved by four times with proper state preparation and the measured SNR has been improved by about three times.

For D_1 transitions in Figs. 3(a) and 3(b), the saturation parameter of the spectroscopy laser is set to be $s = 2(1) \times 10^{-4}$. We obtain the transition $|\uparrow\rangle \rightarrow\ ^2P_{1/2}|3,0\rangle$ by preparing the ion at initial state $|\uparrow\rangle$, and obtain the transition $|\downarrow\rangle \rightarrow\ ^2P_{1/2}|2,0\rangle$ by preparing the ion at initial state $|\downarrow\rangle$. Unlike D_2 transitions, there is only one $m_F = 0 \rightarrow m_F = 0$ transition in the scanning range, so the improper line shape function line pulling effect is smaller than that of D_2 transitions.

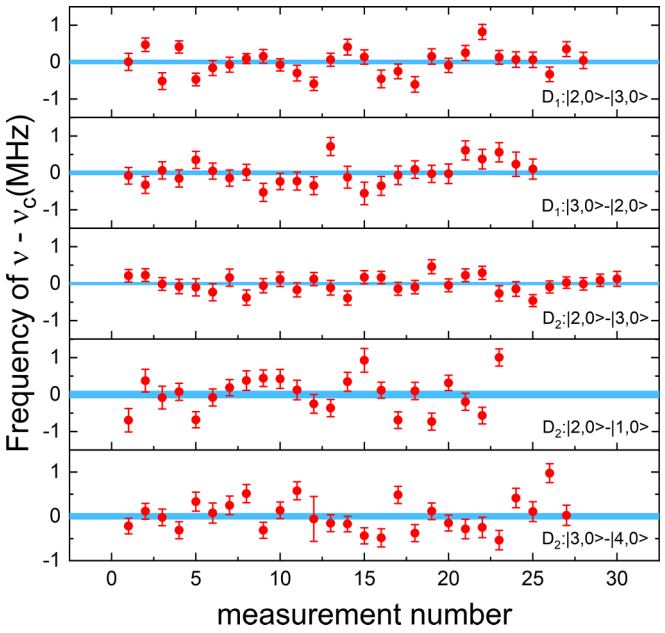

FIG. 4. Hyperfine transition line centroids of the D_1 and D_2 transitions, each of which is measured multiple times in different days. The round points are the fitted line centers and the error bars indicate the statistical uncertainties. All measurements have their average frequencies subtracted out, so blue lines are all centered at zero frequency, with the thickness of each line indicating 1σ statistical uncertainty of the total measurement data.

Each hyperfine structure line is measured multiple times in several days, and their center frequencies are shown in Fig. 4 with the offset frequencies subtracted out. The statistical uncertainties are listed in Table I. For D_1 transitions, ${}^2S_{1/2}\,|2,0\rangle \rightarrow {}^2P_{1/2}|3,0\rangle$ and ${}^2S_{1/2}\,|3,0\rangle \rightarrow {}^2P_{1/2}|2,0\rangle$ have 28 and 25 line scans, respectively. For D_2 transitions, ${}^2S_{1/2}\,|2,0\rangle \rightarrow {}^2P_{3/2}\,|3,0\rangle$, ${}^2S_{1/2}\,|2,0\rangle \rightarrow {}^2P_{3/2}\,|1,0\rangle$ and ${}^2S_{1/2}\,|3,0\rangle \rightarrow {}^2P_{3/2}\,|4,0\rangle$ are measured with 30, 23, and 27 line scans, respectively, and the measurement number of each transition line is $N = 350$.

In Table I, we list all the evaluated systematic uncertainties. The line profiles we measured are the convolution of the laser spectrum and the ion transition [31]. So the asymmetry of the laser spectrum would induce a frequency shift of the probed transitions. To evaluate the asymmetry of the spectrum caused by the correlated amplitude and phase modulation, we fit the beat signal spectrum of the frequency comb and the 1120-nm laser with a Gaussian function and find a 37(6)-kHz deviation between the fitted center and the counted frequency at 1120 nm, in which the deviation induced by the frequency comb is much smaller than 1 kHz. Here, we take the deviation as the upper limit of the systematic uncertainty, and obtain an uncertainty of 0.15 MHz in UV.

The imperfect state preparation will lead to undesired transitions, such as the transition between ${}^2S_{1/2}\,|2,2\rangle$ and ${}^2P_{3/2}\,|2,2\rangle$. We evaluate this effect through numerical simulations [49] and obtain the correlation between the frequency shift and the population distributions. For the imperfect state preparation, the $|\uparrow\rangle \rightarrow {}^2P_{1/2}|3,0\rangle$ transition corresponds to a frequency shift of 0.37(15) MHz. Due to the large frequency difference between the two excited energy levels, the uncertainties in D_1 transitions are smaller than those in D_2. Line pulling effects from the other hyperfine structure levels have been included in the simulations. And the line pulling shifts from the other levels have been evaluated and contained in the imperfect state preparation in Table I. The transition ${}^2S_{1/2}\,|2,0\rangle \rightarrow {}^2P_{3/2}\,|2,0\rangle$ in principle is a forbidden transition, but the impure π polarized light would induce undesired σ transitions. The σ transitions between the Zeeman sublevels would shift the line center. Therefore, we use a half-wave plate and a quarter-wave plate (QWP) to optimize the laser polarization purity [31,42,50]. We rotate the angle of the QWP to minimize the σ transition probability with an uncertainty of 0.02, corresponding to a maximum polarization angle deviation of 4°. The polarization impurity of the spectroscopy laser is evaluated within 2%. We evaluate the frequency shifts due to the polarization impurity through numerical simulations in the Supplemental Material [49], and the results are presented in Table I.

As described before, we stabilize the laser power with a digital locking system and achieve a relative intensity noise below $10^{-2}/\sqrt{\text{Hz}}$ during the laser frequency scanning. The instability of the laser power is suppressed by about one order of magnitude. The duration of each line scan is about 860 s, in which the fluctuation of the laser power at different frequency will cause the asymmetry of the transition lines. We add the power fluctuations into the simulation to obtain a transition line and fit it with a Voigt function to obtain the fitted frequency. The remaining shift is given with the difference between the fitted frequency and the resonant

TABLE I. Summary of the systematic frequency shifts and their uncertainties of the doublet transition frequencies.

	D_1 (MHz)		D_2 (MHz)		
Effect	$\|\downarrow\rangle \rightarrow \|3,0\rangle$	$\|\uparrow\rangle \rightarrow \|2,0\rangle$	$\|\uparrow\rangle \rightarrow \|3,0\rangle$	$\|\uparrow\rangle \rightarrow \|1,0\rangle$	$\|\downarrow\rangle \rightarrow \|4,0\rangle$
Laser spectrum asymmetry	0.00(15)	0.00(15)	0.00(15)	0.00(15)	0.00(15)
Laser polarization impurity	0.00(3)	0.00(4)	0.00(13)	0.00(13)	0.00(15)
Imperfect state preparation	0.08(3)	0.00(3)	0.37(15)	0.76(15)	−2.11(54)
Second-order Zeeman effect	0.00(1)	0.00(1)	0.00(11)	0.00(9)	0.00(6)
Laser relative intensity noise	0.00(5)	0.00(5)	0.00(5)	0.00(5)	0.00(5)
Frequency measurement	0.000(1)	0.000(1)	0.000(1)	0.000(1)	0.000(1)
Statistical	0.00(6)	0.00(6)	0.00(4)	0.00(10)	0.00(7)
Total	0.08(17)	0.00(18)	0.37(28)	0.76(29)	−2.11(59)

TABLE II. Doublet line transition frequencies of $^{25}Mg^{+}$ in this work and their comparison with previous results.

Transitions	Batteiger *et al.* [30]	Clos *et al.* [41]	Ozawa *et al.* [40]	This work
D_1 (MHz)	1 069 339 962(19)	1 069 339 957(5)		1 069 339 961.98(12)
D_2 (MHz)	1 072 084 555(19)	1 072 084 547(5)	1 072 084 553.3(7)	1 072 084 554.77(24)

frequency. With the numerical simulation, the upper limit of the frequency shift is 50 kHz. We measure the laser beam profile at different laser frequencies and do not find obvious laser mode distortion within the tuning range. The relative laser power variation at the maximum frequency offset difference is below 4×10^{-3} [49], which corresponds to an uncertainty of 10 kHz. In total, the uncertainty caused by the laser relative intensity variation is 0.05 MHz. The doublet line transitions we measured are insensitive to the magnetic field because of the Zeeman levels $m_F = 0$, but they still have second-order Zeeman shifts. We evaluate the second-order Zeeman shifts with the Breit-Rabi formula [39], and take these shifts as systematic errors. We list the uncertainties caused by the second-order Zeeman effect in Table I. The frequency of the hydrogen maser is calibrated with a GPS receiver, and contributes a frequency uncertainty of 1 kHz.

For $^{25}Mg^{+}$ ion, the hyperfine splitting can be described by Eqs. (1)–(3). $A_{S_{1/2}}$, $A_{P_{1/2}}$, and $A_{P_{3/2}}$ represent the magnetic dipole constants of ground state $^2S_{1/2}$ and excited states $^2P_{1/2}$ and $^2P_{3/2}$. $B_{P_{3/2}}$ is the electric quadrupole constant. F is the total angular momentum quantum number of the ion, I is the nuclear spin, J is the total angular momentum quantum number of the electron, and $K = F(F+1) - I(I+1) - J(J+1)$. With these equations and the measured hyperfine transition frequencies, we can obtain the doublet line transition frequencies and the hyperfine constants:

$$\Delta E_{S_{1/2}} = \frac{1}{2} h A_{S_{1/2}} [F(F+1) - I(I+1) - J(J+1)] \quad (1)$$

$$\Delta E_{P_{1/2}} = \frac{1}{2} h A_{P_{1/2}} [F(F+1) - I(I+1) - J(J+1)] \quad (2)$$

$$\Delta E_{P_{3/2}} = \frac{1}{2} h A_{P_{3/2}} K + B_{P_{3/2}} \frac{[3K(K+1) - 4I(I+1)J(J+1)]}{8I(2I-1)J(2J-1)} \quad (3)$$

TABLE III. The hyperfine constants (in MHz) of $^{25}Mg^{+}$ ion. With the hyperfine transition frequencies, we calculate the hyperfine structure constants of the low-lying excited state $^2P_{1/2}$ and $^2P_{3/2}$, and compare with the results of other groups.

Group	$A_{P_{1/2}}$	$A_{P_{3/2}}$	$B_{P_{3/2}}$
This work (Exp.)	−102.87(8)	−18.74(9)	24.54(45)
This work (Theor.)	−102.02(94)	−19.46(45)	22.67(32)
Nguyen [36]	−102.16(16)		
Safronova *et al.* [33]	−103.4	−19.29	
Sur *et al.* [34]	−101.70[a]	−18.89[a]	22.91
Mani *et al.* [35]	−102.997	−19.546	

[a]The sign of the nuclear magnetic moment was not properly taken into account in Sur *et al.* [34], so we add an extra minus sign to the result.

In Table II, we list our results and compare them with the results of other groups. The D_1 and D_2 transition frequencies in this work are measured to be 1 069 339 961.98(12) MHz and 1 072 084 554.77(24) MHz, respectively. The doublet frequencies are in good agreement with the recent experimental results [41]. We use the doublet line transition frequencies of $^{24}Mg^{+}$ in Ref. [30] and our results to calculate the isotope shifts between $^{24}Mg^{+}$ ion and $^{25}Mg^{+}$ ion. For D_1 and D_2 transitions, the isotope shifts are 1619.42(20) MHz and 1620.44(29) MHz, respectively, whose uncertainties are reduced by nearly one order of magnitude. We also calculate the theoretical hyperfine structure constants with GRASP2018 [51] using the multiconfiguration Dirac-Hartree-Fock (MCDHF) method [52]. The results of the hyperfine structure constants are shown in Table III, together with the results of other groups. The maximum difference between the measured magnetic dipole constant $A_{P_{1/2}} = -102.87(8)$ MHz and the other groups' results is about 1%. The maximum difference between the measured magnetic dipole constant $A_{P_{3/2}} = -18.74(9)$ MHz and the other groups' results is about 4%, while the maximum difference between the measured electric quadrupole constant $B_{P_{3/2}} = 24.54(45)$ MHz and the theoretical results is about 8%. This indicates that more physical effects might need to be taken into account, such as the possible capture of electron correlations in our theoretical calculation. Detailed information is provided in the Supplemental Material [49].

In conclusion, we obtain the resolved hyperfine transition frequencies of $^{25}Mg^{+}$ ion with the decoherence-assisted method and improve the SNR by proper preparation of the ion's initial states. Since the ion is sensitive to the laser-induced decoherence, we can utilize this characteristic to enhance the weak signal in a quantum system. The uncertainties of the measured frequencies are one third of that in Ref. [40]. It can be used as a reference for the astrophysical spectra and can be used for the study of isotope shift theory. Simultaneously, we give the measured hyperfine structure constants and the theoretical values. To further improve the measurement precision, the initial state preparation and laser polarization purity need to be optimized and the Zeeman sublevel transitions need to be considered in the fitting function to reduce the line pulling effects.

This work is partially supported by the National Key R&D Program of China (Grant No. 2017YFA0304400), the Key-Area Research and Development Program of GuangDong Province (Grant No. 2019B030330001), and the National Natural Science Foundation of China (Grants No. 11774108, No. 91336213, No. 61875065, and No. 12004124). The authors gratefully acknowledge the Beijing Super Cloud Computing Center (BSCC) for providing HPC resources that have contributed to the research results reported in this paper.

[1] M. P. Savedoff, Nature (London) **178**, 688 (1956).
[2] A. M. Wolfe, R. L. Brown, and M. S. Roberts, Phys. Rev. Lett. **37**, 179 (1976).
[3] J. K. Webb, V. V. Flambaum, C. W. Churchill, M. J. Drinkwater, and J. D. Barrow, Phys. Rev. Lett. **82**, 884 (1999).
[4] V. A. Dzuba, V. V. Flambaum, and J. K. Webb, Phys. Rev. Lett. **82**, 888 (1999).
[5] J. D. Prestage, R. L. Tjoelker, and L. Maleki, Phys. Rev. Lett. **74**, 3511 (1995).
[6] K. A. Bronnikov and S. A. Kononogov, Metrologia **43**, R1 (2006).
[7] T. Rosenband, D. B. Hume, P. O. Schmidt, C. W. Chou, A. Brusch, L. Lorini, W. H. Oskay, R. E. Drullinger, T. M. Fortier, J. E. Stalnaker, S. A. Diddams, W. C. Swann, N. R. Newbury, W. M. Itano, D. J. Wineland, and J. C. Bergquist, Science **319**, 1808 (2008).
[8] C. Chin, V. V. Flambaum, and M. G. Kozlov, New J. Phys. **11**, 055048 (2009).
[9] J. C. Berengut and V. V. Flambaum, Hyperfine Interact. **196**, 269 (2010).
[10] J. A. King, J. K. Webb, M. T. Murphy, V. V. Flambaum, R. F. Carswell, M. B. Bainbridge, M. R. Wilczynska, and F. E. Koch, Mon. Not. R. Astron. Soc. **422**, 3370 (2012).
[11] M. T. Murphy and J. C. Berengut, Mon. Not. R. Astron. Soc. **438**, 388 (2013).
[12] J. C. Berengut, V. A. Dzuba, and V. V. Flambaum, Phys. Rev. A **68**, 022502 (2003).
[13] C. Frugiuele, E. Fuchs, G. Perez, and M. Schlaffer, Phys. Rev. D **96**, 015011 (2017).
[14] C. Delaunay, R. Ozeri, G. Perez, and Y. Soreq, Phys. Rev. D **96**, 093001 (2017).
[15] J. C. Berengut, D. Budker, C. Delaunay, V. V. Flambaum, C. Frugiuele, E. Fuchs, C. Grojean, R. Harnik, R. Ozeri, G. Perez, and Y. Soreq, Phys. Rev. Lett. **120**, 091801 (2018).
[16] Y. V. Stadnik, Phys. Rev. Lett. **120**, 223202 (2018).
[17] I. Counts, J. Hur, D. P. L. Aude Craik, H. Jeon, C. Leung, J. C. Berengut, A. Geddes, A. Kawasaki, W. Jhe, and V. Vuletić, Phys. Rev. Lett. **125**, 123002 (2020).
[18] C. Solaro, S. Meyer, K. Fisher, J. C. Berengut, E. Fuchs, and M. Drewsen, Phys. Rev. Lett. **125**, 123003 (2020).
[19] V. A. Yerokhin, R. A. Müller, A. Surzhykov, P. Micke, and P. O. Schmidt, Phys. Rev. A **101**, 012502 (2020).
[20] J. K. Webb, C. Lee, and D. Milaković, Universe **8**, 266 (2022).
[21] M. T. Murphy, P. Molaro, A. Leite, G. Cupani, S. Cristiani, V. D'Odorico, R. G. Santos, C. Martins, D. Milakovic, N. J. Nunes, T. M. Schmidt, F. A. Pepe, R. Rebolo, N. C. Santos, S. G. Sousa, M. Osorio, M. Amate, V. Adibekyan, Y. Alibert, C. A. Prieto *et al.*, Astron. Astrophys. **658**, A123 (2022).
[22] M. T. Murphy, J. K. Webb, and V. V. Flambaum, Mon. Not. R. Astron. Soc. **345**, 609 (2003).
[23] M. G. Kozlov, V. A. Korol, J. C. Berengut, V. A. Dzuba, and V. V. Flambaum, Phys. Rev. A **70**, 062108 (2004).
[24] R. E. Drullinger, D. J. Wineland, and J. C. Bergquist, Appl. Phys. **22**, 365 (1980).
[25] D. J. Wineland and W. M. Itano, Phys. Lett. A **82**, 75 (1981).
[26] W. Nagourney, G. Janik, and H. Dehmelt, Proc. Natl. Acad. Sci. USA **80**, 643 (1983).
[27] D. Goorvitch, G. Mehlman-Balloffet, and F. P. J. Valero, J. Opt. Soc. Am. **60**, 1458 (1970).
[28] J. C. Pickering, A. P. Thorne, and J. K. Webb, Mon. Not. R. Astron. Soc. **300**, 131 (1998).
[29] M. Aldenius, S. Johansson, and M. T. Murphy, Mon. Not. R. Astron. Soc. **370**, 444 (2006).
[30] V. Batteiger, S. Knünz, M. Herrmann, G. Saathoff, H. A. Schüssler, B. Bernhardt, T. Wilken, R. Holzwarth, T. W. Hänsch, and T. Udem, Phys. Rev. A **80**, 022503 (2009).
[31] M. Herrmann, V. Batteiger, S. Knünz, G. Saathoff, T. Udem, and T. W. Hansch, Phys. Rev. Lett. **102**, 013006 (2009).
[32] J. Heully and A. Mårtensson-Pendrill, Phys. Scr. **31**, 169 (1985).
[33] M. S. Safronova, A. Derevianko, and W. R. Johnson, Phys. Rev. A **58**, 1016 (1998).
[34] C. Sur, B. K. Sahoo, R. K. Chaudhuri, B. P. Das, and D. Mukherjee, Eur. Phys. J. D **32**, 25 (2005).
[35] B. K. Mani and D. Angom, Phys. Rev. A **81**, 042514 (2010).
[36] J. Nguyen, The linewidth and hyperfine a constant of the $^2P_{1/2}$ state of a magnesium ion confined in a linear Paul trap, Ph.D. thesis, McMaster University, 2009.
[37] W. M. Itano and D. J. Wineland, Phys. Rev. A **24**, 1364 (1981).
[38] Z. T. Xu, K. Deng, H. Che, W. H. Yuan, J. Zhang, and Z. H. Lu, Phys. Rev. A **96**, 052507 (2017).
[39] S. M. Brewer, J. S. Chen, K. Beloy, A. M. Hankin, E. R. Clements, C. W. Chou, W. F. McGrew, X. Zhang, R. J. Fasano, D. Nicolodi, H. Leopardi, T. M. Fortier, S. A. Diddams, A. D. Ludlow, D. J. Wineland, D. R. Leibrandt, and D. B. Hume, Phys. Rev. A **100**, 013409 (2019).
[40] A. Ozawa, J. Davila-Rodriguez, J. R. Bounds, H. A. Schuessler, T. W. Hansch, and T. Udem, Nat. Commun. **8**, 44 (2017).
[41] G. Clos, M. Enderlein, U. Warring, T. Schaetz, and D. Leibfried, Phys. Rev. Lett. **112**, 113003 (2014).
[42] W. H. Yuan, K. Deng, Z. Y. Ma, H. Che, Z. T. Xu, H. L. Liu, J. Zhang, and Z. H. Lu, Phys. Rev. A **98**, 052507 (2018).
[43] Z. Y. Ma, H. L. Liu, W. Z. Wei, W. H. Yuan, P. Hao, Z. Deng, H. Che, Z. T. Xu, F. H. Cheng, Z. Y. Wang, K. Deng, J. Zhang, and Z. H. Lu, Appl. Phys. B **126**, 129 (2020).
[44] W. Wei, P. Hao, Z. Ma, H. Zhang, L. Pang, F. Wu, K. Deng, J. Zhang, and Z. Lu, J. Phys. B: At. Mol. Opt. Phys. **55**, 075001 (2022).
[45] J. Zhang, X. H. Shi, X. Y. Zeng, X. L. Lü, K. Deng, and Z. H. Lu, Rev. Sci. Instrum. **87**, 123105 (2016).
[46] M. Horbatsch and E. A. Hessels, Phys. Rev. A **82**, 052519 (2010).
[47] T. Udem, L. Maisenbacher, A. Matveev, V. Andreev, A. Grinin, A. Beyer, N. Kolachevsky, R. Pohl, D. C. Yost, and T. W. Hänsch, Ann. Phys. **531**, 1900044 (2019).
[48] W. Ansbacher, Y. Li, and E. H. Pinnington, Phys. Lett. A **139**, 165 (1989).
[49] See Supplemental Material at http://link.aps.org/supplemental/10.1103/PhysRevA.107.L020803 for the details on the numerical simulations and uncertainty evaluations of the doublet transitions, and the theoretical calculations of the hyperfine structure constants.
[50] W. H. Yuan, H. L. Liu, W. Z. Wei, Z. Y. Ma, P. Hao, Z. Deng, K. Deng, J. Zhang, and Z. H. Lu, Rev. Sci. Instrum. **90**, 113001 (2019).
[51] C. F. Fischer, G. Gaigalas, P. Jönsson, and J. Bieroń, Comput. Phys. Commun. **237**, 184 (2019).
[52] C. F. Fischer, M. Godefroid, T. Brage, P. Jönsson, and G. Gaigalas, J. Phys. B: At. Mol. Opt. Phys. **49**, 182004 (2016).